doi: 10.82124/CEAS-GNC-2026-068 CEAS-GNC-2026-068

Post-Capture Detumbling of Satellites: A Combined Robust INDI and MPC Approach

João T. Diz PhD Candidate/GNC Engineer, TU Delft/Indra Deimos, Control & Simulation/GNC Team, 2628 CD/1070-061, Delft/Lisbon, The Netherlands/Portugal. jtmarques@indracompany.com

Afonso Botelho PhD Candidate, Instituto Superior Técnico, Universidade de Lisboa INESC-ID, Lisbon, Portugal Indra Deimos, Lisbon, Portugal. afonso.botelho@tecnico.ulisboa.pt

Paulo Rosa Head of Flight Segment, Indra Deimos, Avenida Columbano Bordalo Pinheiro 75, 1070-061 Lisbon, Portugal. parosa@indracompany.com

Spilios Theodoulis Associate Professor, Technical University of Delft, 2628 CD Delft, Netherlands. s.theodoulis@tudelft.nl

ABSTRACT

The increasing population of defunct satellites and debris in Earth orbit poses a significant threat to the sustainability of future space operations, making active debris removal a critical capability for in-orbit servicing (IOS). A key challenge in such missions is post-capture detumbling, where the combined chaser–target system must be stabilized despite large and uncertain inertia variations, underactuation, and strict actuator limits. This work proposes a novel guidance and control framework that integrates Incremental Nonlinear Dynamic Inversion (INDI), $\mathcal{H}_\infty$ Open Loop Shaping, and Model Predictive Control (MPC) to achieve safe and robust post-capture detumbling. INDI provides real-time linearization and adaptive compensation for modeling errors, while $\mathcal{H}_\infty$ tuning offers formal robustness guarantees, and MPC — whose design is simplified by exploiting the INDI linearization — provides a guidance trajectory that enforces actuator and state constraints while optimizing performance objectives. The approach is validated through nonlinear simulations, demonstrating that the $\mathcal{H}_\infty$-tuned INDI control system can stabilize the satellite stack under large inertia uncertainty but causes transient actuator saturation and large angular rates. In contrast, the combined MPC & INDI framework achieves constraint-compliant detumbling and a decrease in settling time. These results establish a robust and computationally efficient guidance and control solution for post-capture operations and lay the groundwork for future extensions including flexible dynamics and fuel sloshing effects.

Keywords: Incremental Nonlinear Dynamic Inversion, H-infinity Open Loop Shaping, Model Predictive Control, Detumbling

1 Introduction

Space robotic systems are essential for in-orbit servicing (IOS) [1–3], enabling the maintenance, repair, and extension of the operational life of space assets, as well as supporting Europe's autonomous and competitive access to space [4]. The ability of these systems to perform IOS operations is becoming

increasingly critical as the number of satellites in Earth orbit continues to rise, while only a small fraction remain functional at any given time [5, 6]. Non-functional satellites and other debris pose significant risks to active spacecraft and future missions. If left unmitigated, the accumulation of debris could trigger a cascade of collisions — a phenomenon known as the Kessler Syndrome — potentially rendering entire orbital regions unusable. To prevent such catastrophic scenarios, it is not enough to perform collision avoidance with active satellites alone; active debris removal has become a necessary component of sustainable space operations [6].

Among the tasks required for active debris removal, one of the most challenging is handling non-cooperative tumbling satellites. Capture missions of such targets can be divided into two distinct phases [7]. The pre-grasping phase involves maneuvering the servicing spacecraft, during which a manipulator is used to securely grasp the satellite. The post-grasping phase requires the robotic system to actively dissipate the rotational motion of the combined spacecraft and stabilize it for safe manipulation and any subsequent operations. Post-grasping de-tumbling is particularly challenging due to the uncertain mass and inertia properties of the combined system. Additional difficulties arise from under-actuation, complex motion constraints, possible actuator failures, and highly flexible structures, which can exhibit chaotic behavior and further complicate stabilization [8]. Designing control strategies that remain robust under these challenges is therefore critical to ensure safe and effective post-capture operations.

Numerous studies have addressed post-capture de-tumbling of satellites. Time-optimal control strategies have been proposed to minimize stabilization time, often in combination with estimators for the system's mass and inertia properties [7, 9]. Adaptive and robust control approaches have also been developed to handle uncertainties in the system's dynamic properties [10, 11]. Energy-efficient strategies have additionally been investigated to improve de-tumbling performance under mission constraints [12]. A thorough review of existing post-capture de-tumbling solutions is provided in [8]. Recently, linear parameter-varying (LPV) control has attracted attention as an alternative approach for IOS missions [13–16], due to its ability to systematically handle highly varying dynamics while offering formal robustness guarantees.

LPV provides a systematic framework for handling highly varying dynamics, including changes in inertia, flexible motion, and fuel sloshing. Its solid theoretical foundation allows for formal robustness guarantees, which is particularly important for safety-critical spacecraft operations. These advantages make LPV a promising approach for post-capture de-tumbling. However, designing LPV controllers is not trivial, even with existing software tools such as the one described in [17]. Practical implementation can be challenging, as LPV synthesis often produces full-order controllers. Additionally, LPV control requires estimation of scheduling parameters, such as the mass or inertia of the combined system, which may limit its applicability in real missions.

An alternative approach is Incremental Nonlinear Dynamic Inversion (INDI), which has been extensively investigated in recent years [18–21]. INDI is a control technique that seeks to '*cancel out*' the system's nonlinearities through feedback, yielding a closed-loop system with linear input-output behavior and thereby reducing or even eliminating the need for gain-scheduling [22]. By leveraging measurements or estimates of angular acceleration and previous control inputs to perform the inversion, INDI exhibits strong robustness to low-frequency uncertainties [22] and can consequently manage unknown and highly varying dynamics. Moreover, its modular design simplifies development and enhances reproducibility across missions compared to LPV-based approaches. The theoretical foundations and practical application of INDI-based control laws for rigid spacecraft have also been established, accounting for limitations such as the limited bandwidth of spacecraft actuators [18, 23, 24].

Despite its advantages, INDI has traditionally faced a key limitation: as a nonlinear control method, it provides no inherent formal guarantees on robustness or performance. Recent developments have addressed this limitation by enabling INDI control laws to be tuned via $\mathcal{H}_\infty$ Open Loop Shaping (OLS) [25]. Another significant advantage of INDI is that, by effectively linearizing the closed-loop the system

dynamics in real time, it can be combined with optimal control strategies such as linear model predictive control (MPC) without imposing a substantial computational burden. Previous studies have combined NDI (the non-incremental version) with MPC [26–29], and more recently, INDI has been successfully integrated with MPC [30]. This combination works synergetically in a guidance and control architecture, and is particularly appealing for post-capture de-tumbling, where the system must stabilize a tumbling satellite under tight safety and performance requirements. On the one hand, INDI linearizes the system, which is otherwise highly nonlinear due to the attitude dynamics, such that the MPC problem is greatly simplified. On the other hand, MPC provides higher-level trajectory planning that allows for explicit enforcement of actuator and state limits, which, in principle, prevents actuator saturation and ensures that the linearization achieved by INDI is preserved [26]. At the same time, MPC can optimize performance objectives, such as minimizing de-tumbling time or energy consumption over a finite horizon. By combining robustly tuned INDI with MPC, the resulting control strategy is expected to effectively handle uncertainties, flexible dynamics, and partially unknown system properties, achieving efficient and safe post-capture stabilization.

Building on this analysis, the present work proposes a guidance and control framework for post-capture de-tumbling that integrates INDI, $\mathcal{H}_\infty$ OLS, and MPC. The approach exploits the complementary strengths of the three methods: INDI provides real-time linearization and modular design, $\mathcal{H}_\infty$ OLS ensures formal robustness and performance guarantees, and MPC enforces actuator and state constraints while optimizing performance objectives over a finite horizon. The novelty of the proposed framework lies in two key aspects. First, robustly tuned INDI has never been combined with MPC. Second, prior INDI & MPC implementations have been limited to quadrotor systems and have not addressed scenarios with significant uncertainties or unmodeled dynamics. In this preliminary study, the application focuses solely on spacecraft attitude dynamics, modeling the combined system as a rigid body with a very large inertia (unknown to the controller), while neglecting flexible dynamics and sloshing effects. Reaction wheels are considered as the primary actuators, modeled as torque sources with first-order dynamics and saturation limits for simplicity of implementation.

The rest of this work is structured as follows. Section 2 describes the rigid-body spacecraft model. Section 3 presents a general derivation of INDI and its application to the spacecraft dynamics. Section 4 details the tuning of the INDI control law using $\mathcal{H}_\infty$ Open Loop Shaping. Section 5 introduces the design of the guidance system: Section 5.1 describes the Model Predictive Control (MPC) strategy and its integration with the INDI-linearized system, while in Section 5.2 a simplified non-optimal guidance law is also developed to serve as a baseline for comparison. Section 6 presents nonlinear simulations of the three resulting control configurations (INDI only, INDI with baseline guidance, and INDI with MPC) and analyzes their performance. Finally, Section 7 summarizes the main conclusions and outlines directions for future work.

2 Spacecraft Attitude Model

The spacecraft attitude model describes the rotational motion of the spacecraft about its center of mass. In this work, the spacecraft is modeled as a rigid body, and flexible dynamics and fuel sloshing effects are neglected. The model accounts for the rotational kinematics, the rigid-body rotational dynamics, and external perturbations acting on the system.

2.1 Spacecraft Attitude Dynamics

The attitude dynamics of a spacecraft are described by Euler's rotational equation of motion (shown in vector form):

$$M = J\dot{\omega} + \omega \times J \tag{1}$$

where $M \in \mathbb{R}^3$ is the external moment vector, J is the moment of inertia matrix, and $\omega \in \mathbb{R}^3$ is the angular velocity vector. This equation can be rewritten in differential form [18]:

$$\dot{\omega} = J^{-1}S(\omega)J\omega + J^{-1}M, \quad \omega(0) = \omega_0; \tag{2}$$

where:

$$M = \begin{bmatrix} M_1 \\ M_2 \\ M_3 \end{bmatrix}, \quad J = \begin{bmatrix} J_{11} & J_{12} & J_{13} \\ J_{12} & J_{22} & J_{23} \\ J_{13} & J_{23} & J_{33} \end{bmatrix}, \quad \omega = \begin{bmatrix} \omega_1 \\ \omega_2 \\ \omega_3 \end{bmatrix} \tag{3}$$

and where $S(\omega)$ is given by [18]:

$$S(\omega) = \begin{bmatrix} 0 & \omega_3 & -\omega_2 \\ -\omega_3 & 0 & \omega_1 \\ \omega_2 & -\omega_1 & 0 \end{bmatrix} \tag{4}$$

2.2 Attitude Kinematics

In this work the Modified Rodrigues Parameters (MRPs) are used to describe the system kinematics. Although less common than Euler angles or quaternions, MRPs are well suited for spacecraft attitude control as they use only three coordinates [18].

Defining $\sigma = [\sigma_1 \quad \sigma_2 \quad \sigma_3]^T \in \mathbb{R}^3$ as the vector of the MRPs, the kinematic equations take the form:

$$\dot{\sigma} = N(\sigma)\omega, \quad \sigma(0) = \sigma_0 \tag{5}$$

where:

$$N(\sigma) = \frac{1}{2}\left[I_{3\times3} - S(\sigma) + \sigma\sigma^T - \frac{1}{2}(1 + \sigma^T\sigma)I_{3\times3}\right] \tag{6}$$

and $S(\sigma)$ is given by:

$$S(\sigma) = \begin{bmatrix} 0 & \sigma_3 & -\sigma_2 \\ -\sigma_3 & 0 & \sigma_1 \\ \sigma_2 & -\sigma_1 & 0 \end{bmatrix} \tag{7}$$

As discussed in [18], the MRPs relate to the Euler-axis and principle angle through:

$$\sigma = \lambda \tan\left(\frac{\theta}{4}\right) \tag{8}$$

2.3 External Disturbances and Open Loop System

Spacecraft in orbit are subject to various external disturbance torques. Although the magnitudes of these disturbances vary significantly, they are generally much smaller than the torques generated by the spacecraft's attitude control system [18]. The most significant contributions typically arise from the Earth's gravity field (due to its non-spherical mass distribution), atmospheric drag, third-body gravitational effects, solar radiation pressure, and electromagnetic forces [18].

In many cases, these environmental disturbance torques can be approximated as a combination of a constant bias and periodic components along the body-fixed axes [31]. For the purposes of this work, the

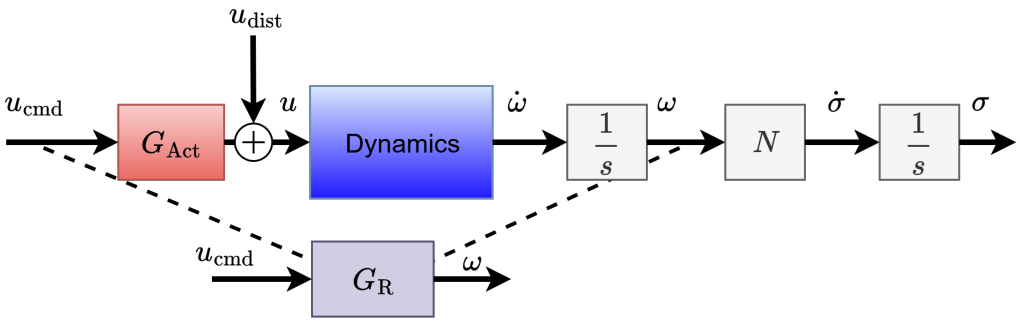

Fig. 1 Open Loop Nonlinear Model.

external disturbance is modeled as a bias plus a sinusoidal torque, expressed as [18, 32]:

$$u_{\text{dist}} = \begin{bmatrix} 4 + 0.2\sin(0.01\pi t) \\ 5 + 0.5\sin(0.01\pi t) \\ 4 + 0.2\sin(0.01\pi t) \end{bmatrix} \times 10^{-3}\,\text{N}\cdot\text{m} \tag{9}$$

and so, the external moment vector is given by:

$$M = u_{\text{dist}} + u_{\text{cmd}} \equiv u \tag{10}$$

where u_{cmd} is the commanded control torque, and u is the input to the spacecraft dynamics.

Figure 1 shows the open-loop nonlinear model. The "Dynamics" block represents the spacecraft rotational dynamics (Eq. 2). The G_{Act} block contains a linear first-order model of the reaction wheels. The $G_{\mathbf{R}}$ block combines both the spacecraft and actuator dynamics while neglecting disturbance inputs. Defining $G_{\mathbf{R}}$ in this way will simplify the explanations in the following sections.

3 Incremental Nonlinear Dynamic Inversion

The underlying idea of Incremental Nonlinear Dynamic Inversion (INDI) is that, through appropriately designed feedback, the system nonlinearities are canceled out, yielding a closed-loop system with linear behavior (under the assumption of perfect inversion). In this linearized framework, a single linear controller can be used to specify the desired performance across the entire flight envelope, thereby eliminating—or at least significantly reducing [22]—the need for gain-scheduling.

While INDI is often described as inherently more robust than NDI (the non-incremental version of INDI), this is only true at low frequencies [22]. At low frequencies, its reduced reliance on the on-board model (OBM) makes the control law less sensitive to modeling errors and parameter variations, improving robustness. At higher frequencies, INDI is less robust because its inherently higher loop gain increases sensitivity to sensor noise and unmodeled dynamics, as per classical control theory (see, e.g., [33], p. 45).

From an implementation standpoint, INDI is generally less demanding than NDI, as it requires only a simplified OBM and does not rely on full state feedback. However, it requires accurate measurements or estimations of actuator deflections and angular accelerations. This shifts the design challenge from maintaining a detailed OBM to ensuring high-quality sensing and filtering, which can introduce practical complications [34].

3.1 Fundamentals of Incremental Nonlinear Dynamic Inversion

Without loss of generality, consider a nonlinear, input affine, multi-input-multi-output system, with m inputs, n states, and the same number of inputs and outputs:

$$\begin{aligned} \dot{x} &= f(x) + g(x)u \\ y &= h(x) \end{aligned} \tag{11}$$

where $u \in \mathbb{R}^m$ represents the control input vector, $x \in \mathbb{R}^n$ represents the state vector, and $y \in \mathbb{R}^m$ is the output vector. $g(x) \in \mathbb{R}^{n \times m}$ is a matrix whose columns are assumed to be smooth vector fields, while, $f(x) \in \mathbb{R}^n$ and $h(x) \in \mathbb{R}^m$ are also assumed to be smooth vector fields.

Starting from nonlinear dynamics of Eq. 11, the control variables are chosen to coincide with the system states so that each output has relative degree one[1] (and, consequently, the system is full-state feedback-linearizable; see [35, 36]). An incremental representation of the system can then be derived by introducing a small time delay λ, as explained below. Define the delayed quantities:

$$\dot{x}_0 = \dot{x}(t-\lambda), \quad x_0 = x(t-\lambda), \quad u_0 = u(t-\lambda) \tag{12}$$

The corresponding increments are then given by $\Delta\dot{x} = \dot{x} - \dot{x}_0$, $\Delta x = x - x_0$, and $\Delta u = u - u_0$, which represent the incremental state derivative, incremental state, and incremental control input, respectively. A first-order Taylor series expansion of $\dot{x}$ with respect to the delay λ is then performed to express the system dynamics in incremental form [19, 21, 37–40]:

$$\begin{aligned} \dot{x} &= \dot{x}_0 + \frac{\partial}{\partial x}\left[f(x) + g(x)u\right]\Big|_{\substack{x=x_0 \\ u=u_0}} \Delta x + g(x_0)\Delta u + H.O.T \\ &= \dot{x}_0 + g(x_0)\Delta u + N(x,\lambda) \end{aligned} \tag{13}$$

where

$$N(x,\lambda) = \frac{\partial}{\partial x}\left[f(x) + g(x)u\right]\Big|_{\substack{x=x_0 \\ u=u_0}} \Delta x + H.O.T \tag{14}$$

which represents a residual term that includes both the Jacobian linearization of the on-board model and the higher-order terms (H.O.T.) arising from the Taylor series expansion.

Assuming that the time delay λ is sufficiently small, the time-scale separation assumption can be applied. This assumption states that the control input u varies much more rapidly than the system states x [19, 21, 37–40]. In practice, this means there is a significant frequency separation between actuator dynamics and vehicle dynamics, which generally holds for aerospace systems [19]. Under this assumption,

$$\Delta x = x - x_0 \approx 0 \tag{15}$$

and, by neglecting the higher-order terms in Eq. 13, the incremental system reduces to [19]:

$$\dot{x} = \dot{x}_0 + g(x_0)\Delta u + \underbrace{N(x,\lambda)}_{\approx 0} \implies \Delta\dot{x} \approx g(x_0)\Delta u \tag{16}$$

Finally, assuming that $g(x_0)$ is invertible in the relevant domain, NDI can be applied to the incremental system. That is, the incremental control input Δu is computed to cancel the effects of $\dot{x}_0$ and $g(x_0)$ in Eq. 16:

$$\Delta u = g(x_0)^{-1}\left[\nu - \dot{x}_0\right] \tag{17}$$

[1] The relative degree of an output corresponds to the number of times the output must be differentiated before the control input explicitly appears into the system dynamics.

The full INDI control input is then obtained by adding the previous actuation signal:

$$u_{\text{INDI}} = u_0 + g(x_0)^{-1} \left[\nu - \dot{x}_0\right] \tag{18}$$

As opposed to the traditional NDI control laws (see [22], for instance), the INDI formulation no longer requires knowledge of the full system dynamics $f(x)$. This significantly reduces sensitivity to modeling errors and facilitates implementation. The resulting control input instead relies on the previous actuation command u_0, the control effectiveness matrix $g(x_0)$, and the measured or estimated state derivative $\dot{x}_0$. Assuming perfect measurement or estimation of these quantities, and that each control variable has relative degree one, the application of the INDI control law to the system in Eq. 16 yields:

$$\frac{y}{\nu} = \frac{1}{s} \tag{19}$$

where ν is the virtual control input. A notable property of this formulation is that it not only linearizes the system, but also decouples the input-output channels [20]. Consequently, each virtual input ν_i influences only the corresponding output y_i, allowing independent control design for each channel.

3.2 Application of INDI to Spacecraft

The first application of INDI to spacecraft was presented in [18], and this work was subsequently extended and refined in [23, 41]. In particular, in [23] an INDI control law for a satellite with reaction wheels was presented and tested. In the present study, however, the inversion of the spacecraft system follows the approach in [18]. Future work will aim to implement the inversion while incorporating the improvements described in the later works.

The inversion strategy described in [18] decomposes the feedback linearization problem into two parts. The first cancels the spacecraft dynamics via INDI, enabling tracking of a desired angular velocity, ω_{des}. The second inverts the spacecraft kinematics, allowing tracking of a specified attitude reference, σ_{des}, and producing the corresponding ω_{des}.

3.2.1 Spacecraft Dynamics Inversion (INDI)

The spacecraft dynamics are canceled using an Incremental Nonlinear Dynamic Inversion control law. Selecting the angular velocity, ω, as the control variable, the INDI law is obtained by substituting the spacecraft-specific quantities into equation 18, resulting in [18]:

$$u_{\text{INDI}} = u_0 + \hat{J} \left[\nu_{\text{in}} - \dot{\omega}_0\right] \tag{20}$$

where quantities with the subscript 0 denote λ-time-delayed variables, ν_{in} is called the inner virtual control input, and $\hat{J}$ is an estimation of the spacecraft's inertia matrix. By applying this law to the system described in Eq. 2, the following relation between virtual input and angular velocity, is obtained:

$$\frac{\omega}{\nu_{\text{in}}} = \frac{1}{s} \tag{21}$$

Figure 2 illustrates the implementation of the INDI law for the inversion of the spacecraft dynamics. Two particular aspects are highlighted. First, since angular acceleration measurements are typically not available in spacecraft, estimation of this variable is required. In this work, a simple first-order derivative filter, denoted H_q, is used to estimate the required quantity. Second, the previous actuator command δ_0 is not directly measured and must therefore be reconstructed. In this work, it is obtained by feeding back the internal Control Command (CC). This approach has been employed in previous studies as a practical alternative when actuator sensor measurements are unavailable [25]. It is straightforward to implement, and recent research suggests that it introduces only minor limitations in terms of control law robustness

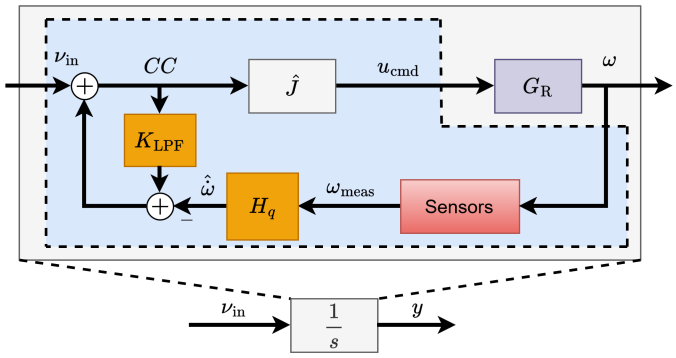

Fig. 2 INDI block-diagram for spacecraft dynamics inversion.

[22]. The CC signal is filtered through a low-pass filter to ensure proper synchronization between the reconstructed actuation feedback and the angular acceleration, as discussed in [42].

3.2.2 Spacecraft Kinematics Inversion (Algebraic Inversion)

As discussed in [18], the spacecraft kinematics describe a purely geometric relationship and can therefore be inverted algebraically. Let the Modified Rodrigues Parameter (MRP) vector, σ, be chosen as the control variable [18]:

$$y = \sigma \tag{22}$$

Differentiating this control variable once yields:

$$\dot{y} = \dot{\sigma} = N(\sigma)\omega \tag{23}$$

This equation describes the kinematic mapping between angular velocity and MRPs and does not involve any modeling uncertainty. As a result, algebraically inverting it is sufficient to define a control law that cancels the kinematic effects [18]:

$$\omega_{\text{des}} = N^{-1}(\sigma)\,[\nu_{\text{out}}] \tag{24}$$

where ν_{out} is the outer virtual control input. This control law generates the desired angular velocity, ω_{des}, and is used to enable tracking of a specified MRP attitude reference.

4 Control Law Design

This section presents the design and tuning of the spacecraft attitude controller adopted in this work. The controller is based on the Incremental Nonlinear Dynamic Inversion (INDI) framework and is tuned using $\mathcal{H}_\infty$ Open Loop Shaping to ensure robustness against model uncertainties and external disturbances. The following subsections describe the structure of the control system, the methodology for tuning via $\mathcal{H}_\infty$ Open Loop Shaping, and the detailed tuning procedure.

4.1 Controller Structure

The controller follows the structure proposed in [18], combining the spacecraft dynamics inversion, the spacecraft kinematics inversion, and two proportional controllers, K_{in} and K_{out}. The proportional controllers, along with the derivative filters and low-pass filters that are part of the INDI law, are implemented independently for each of the three control axes. The overall system and controller architecture is illustrated in Figure 3.

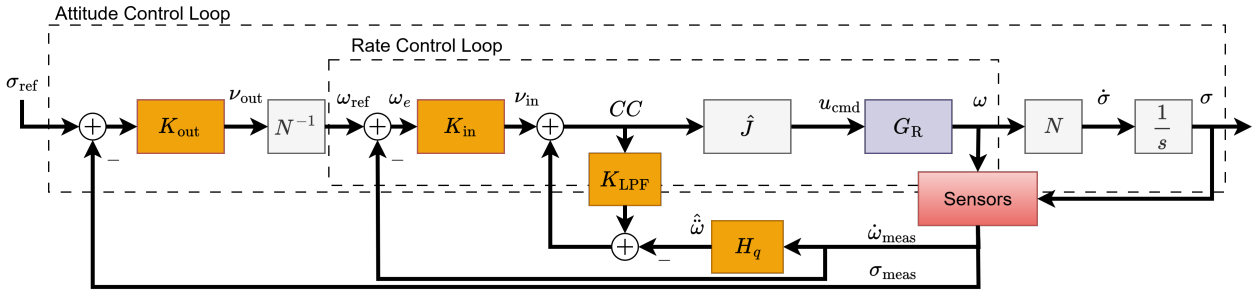

Fig. 3 INDI-based spacecraft block-diagram.

The first proportional controller, K_{in}, is applied in the rate (inner) control loop and governs the angular velocity tracking performance while also contributing to the robustness of the inner loop. The second proportional controller, K_{out}, is part of the attitude (outer) control loop and similarly determines the tracking performance of the attitude reference and the robustness of the outer loop.

4.2 Tuning via $\mathcal{H}_\infty$ Open Loop Shaping

$\mathcal{H}_\infty$ Open Loop Shaping (OLS) is a two-step procedure. First, the open-loop system is shaped using weighting filters (W_1 and W_2) to meet desired performance objectives. Second, the shaped plant ($G_S = W_2 G W_1$) is robustified against Normalized Coprime Factor (NCF) uncertainty. This is accomplished by computing the stabilizing controller that minimizes the $\mathcal{H}_\infty$ norm of the transfer function from a specific four-block problem. Provided that the robustness margin attained in the second step is sufficiently large, the robustification largely preserves the specified loop shape while also providing formal robustness and performance guarantees.

A fundamental requirement of standard $\mathcal{H}_\infty$ Open Loop Shaping is the ability to freely apply weighting filters at both the input and output of the plant. This is incompatible with INDI or other inversion-based controllers, because modifying the plant in this way would interfere with the inversion mechanism and cancel the intended control action. To address this limitation, [25] proposed a dedicated tuning framework which is illustrated by the block diagram shown in Figure 4. In this diagram, G represents the plant, d_i and d_o are the input and output disturbances, u and y are the plant input and output, and K denotes the robust controller, which includes all elements acting on the plant. By selecting appropriate weighting filters (W_1 and W_2), and tuning the controller to minimize the $\mathcal{H}_\infty$ norm of the transfer matrix $T_{w_1,w_2 \to z_1,z_2}$, the loop gains of the system ($L_o = KG$, $L_i = GK$) will converge to those of G_S, the desired shaped plant [2]. At the same time, the standard robustness and performance guarantees of $\mathcal{H}_\infty$ Open Loop Shaping are attained *without affecting the inversion-based structure*.

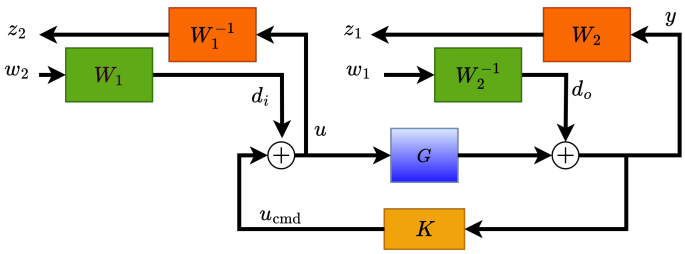

Fig. 4 $\mathcal{H}_\infty$ OLS tuning block-diagram for fixed structure controllers.

[2] This result holds provided that the robustness margin obtained through the tuning process is sufficiently high.

4.3 INDI Controller Tuning Procedure

The INDI-based controller is tuned by applying the approach of Figure 4 to the INDI-based control architecture shown in Figure 3. The resulting tuning configuration is illustrated in Figure 5. In this block-diagram, two sets of outputs are considered: the angular velocity vector ω and the attitude representation vector σ (MRPs). Both outputs are included because robustness is required at two levels: the inner loop, where ω is tracked, and the outer loop, where σ is tracked. By accounting for both simultaneously, the tuning ensures that robustness and performance guarantees extend to both angular velocity and attitude outputs. The input of the tuning block-diagram is placed immediately before the block $G_{\mathbf{R}}$ (i.e., before the combined actuator and spacecraft dynamics), so as to ensure robustness at the plant's input.

Having established the tuning configuration, the system is linearized around the nominal operating conditions, with all states set to zero and the spacecraft inertia at its nominal value[3]. This provides the linear approximation required for $\mathcal{H}_\infty$ controller design. The next step is the selection of appropriate weighting filters, which is performed by analyzing the singular values of the open-loop system. Once the fundamental limitations of the baseline loop shape are identified, the guidelines from [43] are applied to choose the filters. Following this procedure, the resulting set of weighting functions is given by:

$$W_{11} = \frac{s + 0.15}{s} \cdot 3.9, \quad W_{12} = \frac{s + 0.15}{s} \cdot 3, \quad W_{13} = \frac{s + 0.15}{s} \cdot 3.3, \quad W_2 = I_{6\times 6}. \tag{25}$$

The proportional–integral (PI) filters are used to set the system bandwidth at approximately 0.5 rad/s (through the proportional gain), and specify integral action to ensure low-frequency disturbance rejection and zero steady-state tracking error. The zero of each PI filter is placed just below the desired crossover to counteract the phase lag introduced by the integral term and help bring the open-loop slope near crossover closer to -20 dB/dec, as is often desired for robustness [33]. The post-compensator W_2 is kept as the identity matrix. With the weighting filters selected, $\mathcal{H}_\infty$ synthesis is then used to simultaneously tune the proportional controllers K_{out} and K_{in}, the derivative filters H_q, and the low-pass filters K_{LPF}. The resulting controller is denoted K_{INDI} and will be tested in Section 6.

5 Guidance Design

The INDI controller designed in Section 4 tracks a given attitude reference σ_{ref}. By appropriately selecting this reference, the controller can be re-used in different attitude control modes, such as pointing,

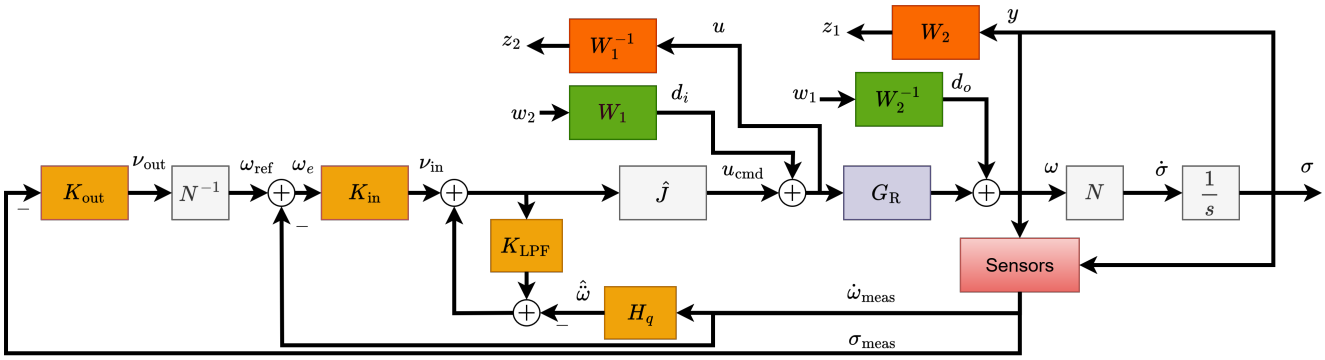

Fig. 5 $\mathcal{H}_\infty$ OLS tuning block-diagram for the INDI-based control law.

[3] Although the system is linearized about a nominal inertia, this does not conflict with the objective of handling inertia uncertainty. INDI relies on measurements or estimated quantities and inherently reduces sensitivity to inaccuracies in the system dynamics. The main limitation lies in the control effectiveness, which can be mitigated by tuning the controller over a representative range of inertia values; a systematic treatment of this aspect is left for future work.

slewing, and detumbling. For maneuvers with large angular displacements, however, the controller may behave undesirably if the reference attitude σ_{ref} is abruptly changed to the final desired attitude σ_{des} (i.e., a large input step signal), potentially causing a long and inefficient transient response as well as actuator saturation, which may degrade the INDI assumptions. This motivates the use of a guidance function to provide a time-varying and smooth attitude reference σ_{ref} that accounts for higher-level considerations, such as manoeuvre efficiency, safety, and actuator saturation, and which ultimately achieves the desired attitude σ_{des}.

We propose a guidance function based on Model Predictive Control, described next in Section 5.1. As a simpler baseline approach for comparison, we also consider in Section 5.2 a feedforward guidance based on filtering the desired attitude σ_{des}.

5.1 Model Predictive Control

Model Predictive Control (MPC) [44] is a powerful nonlinear control method which has in recent decades gained much popularity for autonomous vehicle applications [45], since it allows for the optimization of a desired metric — e.g., fuel, control energy — and for setting explicit constraints that can model control limitations and safety restrictions within a desired time-horizon. Therefore, in comparison to any linear control method, MPC enables higher-level control decision-making, i.e., it can directly account for mission objectives and system and operational limitations, and it thus has the potential to improve the performance, efficiency, safety, and autonomy of space missions and vehicles.

On the downside, MPC requires recursively solving an optimization problem onboard and in real-time, which may be prohibitive in face of the limited computational power available onboard, especially for space applications that demand a radiation hardened onboard computer. Furthermore, such applications are often subject to strict onboard software design requirements, especially in safety critical scenarios, whereby the GNC functions must be guaranteed to successfully compute the output in the allotted timeslot, which is often not possible to ensure for numerical optimization algorithms. Moreover, the current industrial practice and state of the art in control design for space GNC is still reliant on linear stability and frequency analysis tools, which is incompatible with MPC, being a nonlinear control method, having to rely instead on Lyapunov theory. These issues are further compounded if an adequate linearized model is not available for the system to be controlled, thus demanding the use of Nonlinear MPC (NMPC) — which further complicates the attainment of stability and robustness guarantees — and non-convex optimization, which generally has no guarantees of convergence to a (local) optimum.

For these reasons, the practical application of this methodology in aerospace GNC has been mostly limited to missions that have a strict demand for it as an enabling technology, most notably the powered descent and landing of a reusable launch vehicle [46]. On the other hand, due to the above-mentioned limitations, even in such applications onboard optimization is typically used for trajectory generation, i.e., for implementing the guidance function, rather than for directly providing low-level control decisions. Thus, it provides the reference signal to a lower-level linear control system. Nonetheless, periodic but lower-frequency re-computations may still be necessary for updating the guidance reference trajectory in the presence of disturbances and uncertainties that cannot be fully compensated for by the lower-level controller, thus recovering an MPC, albeit used as an outer control-loop, namely closed-loop guidance. This type of layered multirate control architecture has been shown to be very effective in practice [47], combining the flexibility and higher-level trajectory planning of online optimal control with the simplicity and stability/robustness guarantees of linear control.

In this work, we propose such a guidance and control (G&C) framework based on MPC and INDI, respectively. This differs from a typical G&C architecture in that the INDI controller is also nonlinear, although due to recent advances [25], it can be tuned to boast the formal guarantees usually associated with linear robust control methods. Furthermore, the joint use of INDI and MPC can be synergized to great effect. On the one hand, the linearization performed by the INDI can be exploited to simplify

the MPC problem by considering a model of the closed-loop system, which is nominally approximately linear, rather than the open-loop nonlinear dynamics. On the other hand, this simplified MPC can be run at a higher frequency than otherwise possible, to improve performance with respect to disturbances and uncertainty, ensuring that the low-level INDI controller can satisfy the relevant constraints, namely the control authority, which, if saturated, could disrupt the INDI assumptions.

5.1.1 Nonlinear MPC

A standard trajectory optimization approach for generating a guidance trajectory for (11) is to solve an open-loop optimal control problem of the form [45, 48]

$$\min_{u,t_\mathrm{f}} \quad V_\mathrm{f}(x(t_\mathrm{f}), t_\mathrm{f}) + \int_{t_0}^{t_\mathrm{f}} \ell(x(t), u(t), t)\mathrm{d}t \tag{26a}$$

$$\text{s.t.} \quad x(t_0) = \hat{x}(t_0) \tag{26b}$$

$$\dot{x} = f(x) + g(x)u, \qquad \forall t \in [t_0, t_\mathrm{f}] \tag{26c}$$

$$(x(t), u(t)) \in \mathbb{C}, \qquad \forall t \in [t_0, t_\mathrm{f}] \tag{26d}$$

$$x(t_\mathrm{f}) \in \mathbb{X}_\mathrm{f}, \tag{26e}$$

where t_0 is the initial time, t_f the (free) final-time, $\hat{x}$ is the state-estimate, V_f and ℓ are the terminal and stage costs, which may encode higher-level objectives such as control effort minimization, and $\mathbb{C}$ and $\mathbb{X}_\mathrm{f}$ are the path and terminal constraint sets, which typically encode control authority limitations, safety restrictions, and the desired terminal configuration. The output to (26) is thus an optimal and constrained open-loop control profile $u(t)\ \forall t \in [t_0, t_\mathrm{f}]$, and the respective trajectory $x(t)$ can be used as a guidance reference to a closed-loop controller, such as the INDI controller described in Section 4. Alternatively, the optimal control $u(t)$ can be applied directly to the plant for a pre-determined duration, after which the problem is re-computed and the process repeated periodically with an updated state estimate to introduce feedback, which is, of course, the MPC approach [44]; more specifically, problem (26) yields an NMPC due to the nonlinear dynamic model (26c). On the other hand, the standard MPC approach is to pre-determine the temporal horizon $t_\mathrm{f} - t_0$ such that t_f is fixed for each optimization and incremented by the sampling interval with every re-computation, in what is known as *receding-horizon* control.

The optimal control problem (26) is most commonly solved with the direct method, which yields a finite-dimensional nonlinear programming (NLP) problem that can be solved with readily available optimization algorithms [44, Ch. 8]. The resulting problem, however, is inherently non-convex, even for convex constraint sets $\mathbb{C}$ and $\mathbb{X}_\mathrm{f}$ and cost functions $\ell\ \Phi$, due to the nonlinear dynamic constraints (26c). It can thus be computationally challenging to solve it (even locally) with sufficient reliability and efficiency to enable onboard and real-time recursive deployment in a typical satellite onboard computer. This limitation can be lessened if (26) is solely used as a guidance function for another controller rather than a NMPC controller itself, since the required frequency for re-optimizations is reduced or even null. On the other hand, for problems with significant disturbances or uncertainty, as is the case of the detumbling problem considered in this work, periodic recomputations may still be required as in an NMPC, with a required frequency that is potentially incompatible with the computational burden associated. Furthermore, the fact that the manoeuvre starts at a transient state — tumbling uncontrollably — makes it particularly susceptible to computational delays, even if a single initial trajectory computation was solely required.

This computational issue is most often overcome by the use of linearized dynamic models, yielding a much more agreeable Linear MPC problem, although this is not always a feasible approach. Namely, attitude dynamics and kinematics are inherently highly nonlinear, even in the absence of non-rigid-body dynamics like sloshing and flexible modes. While in standard control design this issue can be overcome via linearization about a reference trajectory, this approach is not possible for (26) since it seeks to design

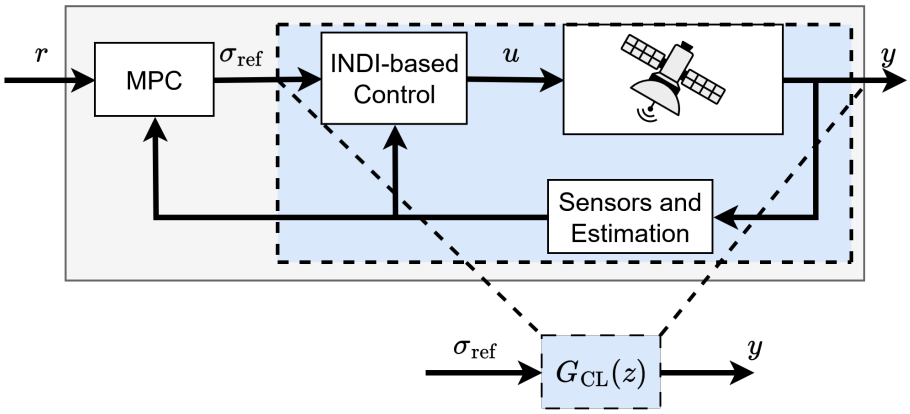

Fig. 6 Block diagram illustrating the integration of the INDI-based control system and the MPC guidance law.

the reference trajectory itself, and it is thus unavailable offline. Optimization methods such as Successive Convexification [48] and Sequential Quadratic Programming [49] work by successive linearization of the dynamics about the solution of the previous iteration, but are still subject to the need to converge to a point that satisfies the original nonlinear dynamics, and the challenges that brings in terms of theoretical guarantees of convergence to an optimum. Therefore, we next propose an alternative approach that can enable the use of Linear MPC for such problems.

5.1.2 INDI-MPC

In ideal conditions where the OBM exactly matches the real plant and the measurements/estimations are perfect, an INDI controller accurately cancels the nonlinearities of the system (11). In that case, any mismatches are due to the neglect of higher-order terms in (13) and the time-scale separation assumption, which can be negligible as discussed in Section 3.1. Therefore, although the plant and controller are nonlinear, the *closed-loop* system G_{CL} is readily approximately linear in nominal conditions. Discretizing $G_{\text{CL}}(s) \xrightarrow{\Delta t} G_{\text{CL}}(z)$, an accurate linearised discrete-time model of the closed-loop system can be obtained, given in state-space by

$$\bar{x}_{k+1} = A\bar{x}_k + B\bar{u}_k, \tag{27}$$

where $k \in \mathbb{N}$ is the discrete time-step, with an augmented state vector $\bar{x} \coloneqq (x, z)$ that includes the controller internal states $z \in \mathbb{R}^{n_c}$, and where the new virtual input variable $\bar{u}$ is the INDI controller reference.

An MPC can be designed for the closed-loop system (27) with the INDI controller rather than for the open-loop nonlinear plant (11), which yields a linear dynamic constraint that is an accurate approximation of the non-convex constraint (26c). Naturally, this simplification assumes the ideal conditions under which the INDI linearization is exact, but typical guidance trajectory optimization approaches also assume a *nominal* model in (26c) [48]. Robust MPC approaches can account for disturbances and uncertainty to ensure robust stability, constraint satisfaction, and recursive feasibility; indeed, the most successful approach in practical application is Tube-Based MPC [44, Ch. 3], which, similarly to (26), optimizes a nominal open-loop trajectory, but with tightened constraints (26d) and (26e) computed offline from a model of the disturbances/uncertainties and from a state-feedback linear controller designed to approximate the true closed-loop action of the MPC. Therefore, the underlying assumption of nominal conditions permitting the use of (27) for designing an MPC as a closed-loop guidance function for the INDI controller is not necessarily more prohibitive than that in standard MPC design. The proposed G&C architecture with the combined MPC-INDI scheme is illustrated in (Fig. 6).

The main downside in the use of the closed-loop model (27) as the MPC prediction model is that the original control variable u is no longer the control decision variable, and is indeed not generally available as a linear function of the augmented state vector $\bar{x}$ and the new input variable $\bar{u}$, which is undesirable given that it is often desirable to minimize u in the cost (26a) and to saturate it in the path constraints (26d). Therefore, the use of the closed-loop INDI-linearized model (27), as opposed to the original nonlinear model (11), appears to have shifted the non-convexities of problem (26) from the dynamic constraints to the cost and constraints. Nonetheless, for an optimization algorithm point-of-view, the latter formulation can be more favorable. Furthermore, in ideal conditions, we can consider a linearized model for the control u of the form

$$u_k = C\bar{x}_k + D\bar{u}_k, \tag{28}$$

which, similarly to (27), has shown to remain quite accurate in numerical examples. The aforementioned Robust MPC methods can then be used to ensure the robust constraint satisfaction despite the linearization and uncertainties, although this was not yet done in the present work.

Considering the closed-loop INDI-linearized and discretized models (27) and (28) in problem (26) yields the MPC problem

$$\begin{aligned}
\min_{\bar{\mathbf{x}},\bar{\mathbf{u}}} \quad & \bar{V}_\mathrm{f}(\bar{x}_N) + \sum_{t=0}^{N-1} \bar{\ell}_k(\bar{x}_k, \bar{u}_k) && && \text{(29a)}\\
\text{s.t.} \quad & x_0 = \hat{x}_0,\ z_0 = \hat{z}_0, && && \text{(29b)}\\
& \bar{x}_{k+1} = A\bar{x}_k + B\bar{u}_k, && \forall k \in \mathbb{N}_{[0,N-1]} && \text{(29c)}\\
& (x_k, C\bar{x}_k + D\bar{u}_k) \in \mathbb{C}, && \forall k \in \mathbb{N}_{[0,N-1]} && \text{(29d)}\\
& x_N \in \mathbb{X}_\mathrm{f}, && && \text{(29e)}
\end{aligned}$$

where $N \in \mathbb{N}$ is the prediction horizon, $\bar{\mathbf{x}} = (\bar{x}_0, \dots, \bar{x}_N)$, $\bar{\mathbf{u}} = (\bar{u}_0, \dots, \bar{u}_{N-1})$, and where the new cost functions $\bar{V}_\mathrm{f}$ and $\bar{\ell}_k$ should include the original objective (26a), with $\ell(\cdot,\cdot,t)$ discretized into $\ell_k(\cdot,\cdot)$, as well as additional terms dependent on z and $\bar{u}$ designed to shape the MPC performance and that of the full G&C.

5.1.3 Application to Detumbling

We next specify the design of the MPC (29) for the detumbling problem addressed in Section 6 and used as a guidance function for the INDI controller K_INDI described in Section 4. The original control variable is the torque u and the original state vector x is the attitude σ and angular velocity ω, i.e., $u = T$ and $x = (\sigma, \omega)$, while the additional states z in G_CL are those of the low-pass filter K_LPF and the derivative filter H_q. Furthermore, z also includes σ_ref, such that the virtual input $\bar{u}$ in the MPC model (27) is the time-derivative of the reference attitude $\dot{\sigma}_\mathrm{ref}$, where (27) is thus obtained by discretizing $G_\mathrm{CL}(s)\frac{1}{s}$, namely with a zero-order hold parametrization of $\dot{\sigma}_\mathrm{ref}$, and with a sampling period Δt assumed to be higher than that of the controller. The adoption of $\dot{\sigma}_\mathrm{ref}$ for $\bar{u}$ rather than directly σ_ref is done for two reasons: 1) enables a smoother reference σ_ref for the controller in-between MPC samples, namely it becomes piecewise affine in continuous-time rather than piecewise constant; 2) enables a smoother overall reference profile σ_ref, by penalizing the virtual input variable $\bar{u} = \dot{\sigma}_\mathrm{ref}$ in the cost function.

The desired guidance path constraints for the original state x and control u variables are

$$\mathbb{C} = \{(x,u) \in \mathbb{R}^6 \times \mathbb{R}^3 : |\omega| \le \omega_\mathrm{max}, |T| \le T_\mathrm{max}\}, \tag{30}$$

while the terminal constraint is

$$\mathbb{X}_\mathrm{f} = \{x \in \mathbb{R}^6 : \sigma = \sigma_\mathrm{des}, \omega = 0\}. \tag{31}$$

The original cost function (26a) is designed to mainly penalize the torque profile u to reduce the control effort, albeit not with a typical fuel-optimal objective since that often yields discontinuous control profiles for which the resulting guidance trajectory would be challenging to track. Therefore, the torque is penalized quadratically, and the cost also includes quadratic regularization terms on the remaining state variables, which yields

$$\ell_k(x,u) = \left\| R_k^{1/2} T \right\|_2^2 + \left\| Q_\sigma^{1/2} (\sigma - \sigma_{\text{des}}) \right\|_2^2 + \left\| Q_\omega^{1/2} \omega \right\|_2^2, \tag{32}$$

where R_k penalize more heavily torque actions at the beginning of the detumbling manoeuvre, at which the models (27) and (28) are less accurate due to the greater angular velocities. On the other hand, the terminal state cost is $V_\text{f}(x) = 0$, since the terminal state is already equality-constrained with (31).

The augmented cost function (29a) penalizes σ_ref and its derivative to favor a slow and smooth reference for the controller to follow, yielding the stage cost

$$\bar{\ell}_k(\bar{x},\bar{u}) = \ell_k(x, C\bar{x} + D\bar{u}) + \left\| Q_\text{ref}^{1/2} (\sigma_\text{ref} - \sigma_\text{des}) \right\|_2^2 + \left\| R_\text{ref}^{1/2} \dot{\sigma}_\text{ref} \right\|_2^2. \tag{33}$$

On the other hand, the augmented terminal cost $\bar{V}_\text{f}$ is also 0. Given that the constraints (30) and (31) are linear and the cost (33) quadratic, the resulting MPC optimization is a quadratic programming (QP) problem.

5.2 Feedforward Guidance Design

In Section 5.1, an MPC-based guidance system was designed. This system generates reference trajectories that ensure all objectives—namely, attitude tracking while satisfying system constraints—are fulfilled. In the specific case of detumbling an uncooperative target with a very large combined spacecraft inertia (as will be tested in the next section), the MPC produces a less aggressive reference command. This allows the controller to achieve the desired final attitude while remaining within the prescribed constraints.

To ensure a fair comparison between the standalone INDI controller and the INDI & MPC configuration, a feedforward (FF) guidance element is introduced. This feedforward controller acts as a simplified guidance system, generating smoother and slower reference commands for the INDI controller.

In this work, the feedforward controller is implemented as a first-order command prefilter (H_{FF}), placed as shown in Figure 7. The filter has the form:

$$H_{FF} = \frac{1}{\tau s + 1} \tag{34}$$

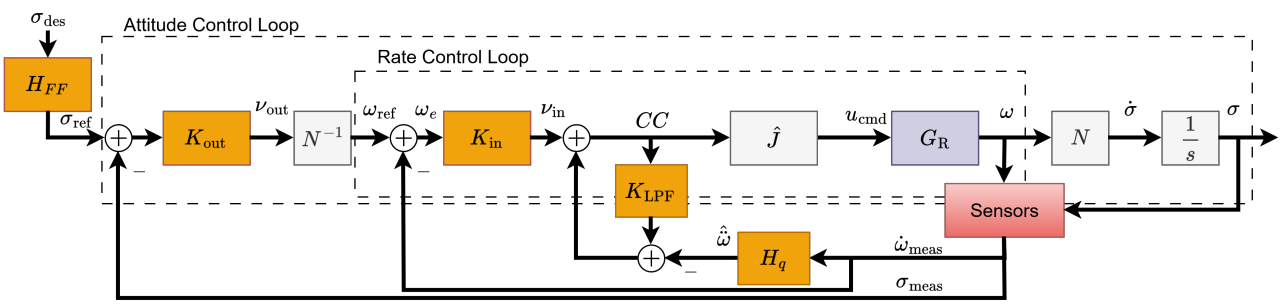

Fig. 7 INDI & Feedforward spacecraft guidance and control block-diagram.

where τ is selected such that the INDI & FF and INDI & MPC systems exhibit near identical settling times in the near-nominal simulation described in Section 6.1.

6 Guidance & Control - Analysis and Result Discussion

This section presents an evaluation of the proposed guidance and control framework for post-capture detumbling. Three strategies are compared: the robustly tuned INDI controller (K_{INDI}), the combined INDI & MPC system ($K_{\text{INDI-MPC}}$), and the combined INDI & FF system ($K_{\text{INDI-FF}}$). The assessment is carried out through nonlinear time-domain simulations in two representative scenarios. In both cases, the control objective is to cancel the initial angular velocity and achieve a desired target attitude.

In the first scenario, simulations are performed using the nominal inertia matrix — the same matrix used for controller tuning — while introducing moderate uncertainties in the inertia elements. This setup allows evaluating the controllers' robustness and performance around the nominal operating conditions. In the second scenario, no uncertainty is considered, and a large bias is applied to the inertia matrix. This configuration is intended to emulate a realistic post-capture scenario by modeling the combined chaser–target system as a spacecraft with significantly increased inertia. The latter simulation is repeated for two different biases.

The controller requirements and performance metrics are summarized in Table 1. The first two requirements are based on the work of [18], while the remaining two specify capabilities that are particularly relevant for post-capture detumbling operations.

For all simulations, the nominal inertia matrix of the spacecraft is defined as [18]:

$$J_{\text{nom}} = \begin{bmatrix} 10 & 0 & 0 \\ 0 & 6.3 & 0 \\ 0 & 0 & 8.5 \end{bmatrix} \text{kgm}^2, \tag{35}$$

and the initial attitude and angular velocity are specified as:

$$\sigma_0 = \begin{bmatrix} 0.05; 0.09; -0.02 \end{bmatrix}, \quad \omega_0 = \begin{bmatrix} 0.02; 0.01; 0.02 \end{bmatrix} \text{ rad/s} \tag{36}$$

Moreover, the final desired conditions for all simulations are given by:

$$\sigma_{\text{des}} = \begin{bmatrix} 0.1; 0.1; 0 \end{bmatrix}, \quad \omega_{\text{des}} = \begin{bmatrix} 0; 0; 0 \end{bmatrix} \text{ rad/s} \tag{37}$$

Table 1 Simulation and control requirements for post-capture detumbling.

Requirement	**Value / Specification**
Angular velocity magnitude	$\|\|\omega\|\| \leq 0.04$ rad/s
Control torque	$T \leq 0.1$ Nm
Attitude tracking	Must track commanded attitude angles, achieving zero steady-state error while constraining the transient response in terms of overshoot and maximum rate
Disturbance rejection	Must be capable of rejecting external disturbances and compensate for changes in the spacecraft inertia

Sensor noise is included in all simulations, modeled as zero-mean Gaussian white noise added to the closed-loop system. The standard deviations are set to $s_{d\sigma} = 1 \times 10^{-3}$ for the attitude vector σ, and $s_{d\omega} = 1 \times 10^{-6}$ rad/s for the angular velocity ω, following the specifications in [18].

The MPC sampling time is $\Delta t = 1$ s and the prediction horizon is $N = 60$, corresponding to a temporal prediction horizon of 60 s. The cost matrices in (32) and (33) were manually tuned to improve the overall G&C performance, and their values are $R_k = r_k I$ with r_k varying linearly with $k \in [0, N-1]$ from $r_0 = 100$ to $r_{N-1} = 5$, $Q_\sigma = 0.1I$, $Q_\omega = 0.01I$, $Q_{\text{ref}} = 10$, and $R_{\text{ref}} = 2000$. The resulting QP problem is solved with MOSEK [50] via its MATLAB interface and using the default solver settings. The MPC is operated with a shrinking-horizon approach, as opposed to the typical receding-horizon, meaning that the prediction horizon N is decremented at each re-computation; the reason behind this design decision is that the cost disproportionately penalizes the torque effort, which, together with a receding-horizon, would cause the MPC to systematically delay the attainment of the terminal configuration at each re-computation, potentially requiring far more than the initially-planned 60 seconds. On the other hand, the shrinking-horizon strategy raises issues of feasibility as the horizon shrinks enough, for which reason the MPC loop is only closed until 45 seconds, after which the remaining reference is tracked in open-loop.

6.1 Near-Nominal Performance

In the near-nominal performance scenario, the perturbed inertia matrix is defined as

$$J_{\text{pert}} = J_{\text{nom}} + \Delta J, \quad \Delta J = \begin{bmatrix} 0.2\,J_{11} & 0.2\,J_{11} & 0.2\,J_{22} \\ 0.2\,J_{11} & 0.2\,J_{22} & 0.2\,J_{33} \\ 0.2\,J_{22} & 0.2\,J_{33} & 0.2\,J_{33} \end{bmatrix} \tag{38}$$

Using this inertia matrix, 100 Monte Carlo simulations were performed, and the results are shown in Figure 8. In terms of MRPs (Fig. 8a), K_{INDI} exhibits the fastest settling time, while the other two controllers show similar settling times. All controllers display comparable dispersion under uncertain conditions. Regarding angular velocity (Fig. 8b), $K_{\text{INDI-MPC}}$ achieves the lowest peak values, as expected from the MRP results, and is the least affected by the dispersed conditions. Nonetheless, all three controllers satisfy the angular velocity limits.

In terms of applied torque (Fig. 8c), the MPC-based controller clearly uses the least torque, followed by $K_{\text{INDI-FF}}$ and then K_{INDI}. The latter exhibits some instances of actuator saturation. Table 2 presents the integral of the torque used by each control strategy over the first 60 s of simulation[4]. The results clearly demonstrate a substantial reduction in control effort when using the INDI-MPC approach. Nonetheless, all three controllers demonstrate strong robustness under uncertainty, with $K_{\text{INDI-MPC}}$ showing the smallest dispersion across the Monte Carlo runs.

Furthermore, the MRP plot indicates that the $K_{\text{INDI-MPC}}$ response closely matches the initial prediction from the linearised MPC model. This confirms that the INDI-linearized predictive model used in the MPC optimization is valid, and that INDI's linearization remains accurate throughout the tested conditions.

Table 2 Comparison of the integrated torque magnitude for each guidance and control strategy across the different simulation scenarios.

G&C Strategy	Near-Nominal (Nms)	Post-Capture Bias 1 (Nms)	Post-Capture Bias 2 (Nms)
K_{INDI}	2.80	4.69	29.6
$K_{\text{INDI-FF}}$	2.50	3.63	9.31
$K_{\text{INDI-MPC}}$	0.88	1.46	2.11

[4]For the Near-Nominal simulation the results pertain the nominal case.

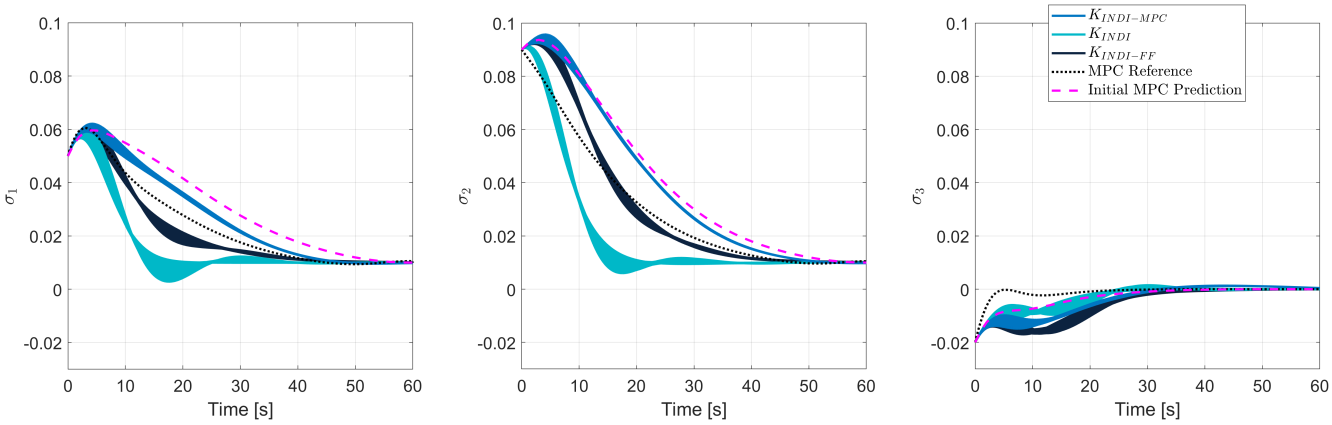

(a) Modified Rodrigues Parameters.

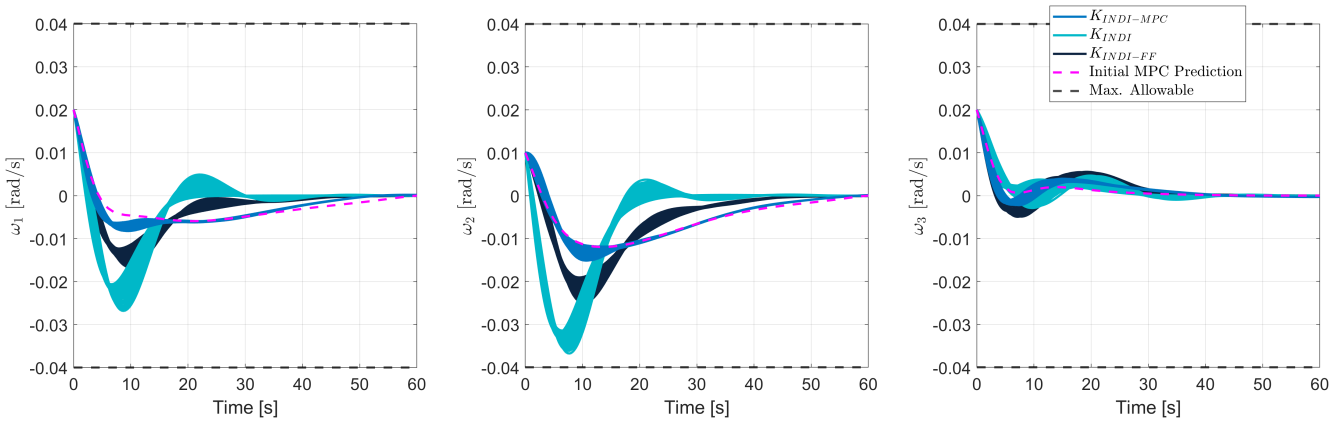

(b) Angular Velocity.

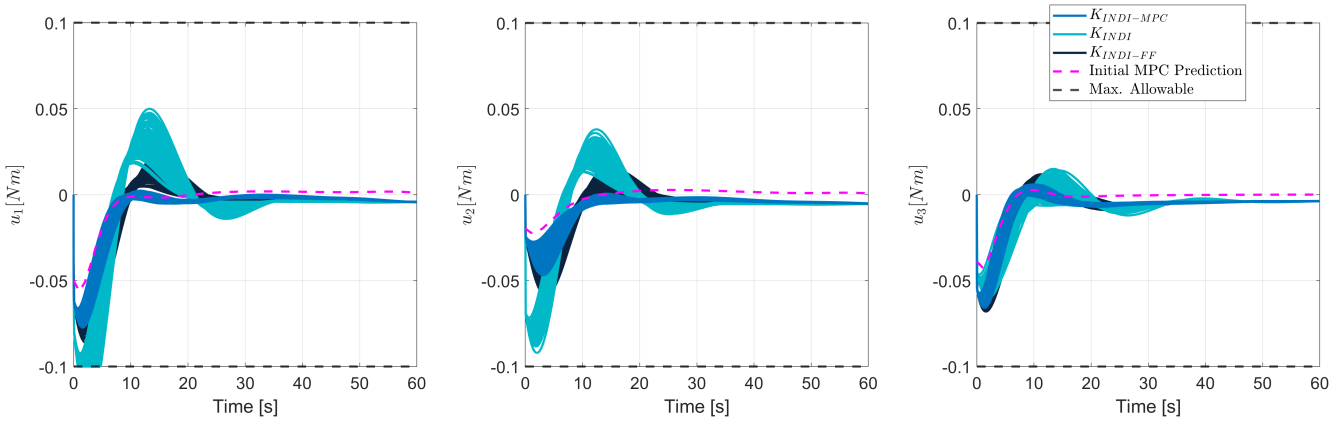

(c) Torque.

Fig. 8 Near-nominal conditions attitude tracking.

The only major discrepancy between the prediction model and the actual realized values occurs in the torque profile; however, this is mainly attributed to the disturbance bias described in Section 2.3.

6.2 Post-Capture Detumbling

This section presents the results of the detumbling simulations for two distinct large inertia matrix biases.

6.2.1 First Post-Capture Detumbling

For the first post-capture detumbling scenario, the inertia matrix is set as:

$$J_{\text{det}} = J_{\text{nom}} + J_{\text{bias}}, \quad J_{\text{bias}} = \begin{bmatrix} J_{\text{nom},11} & 0.2\,J_{\text{nom},11} & 0.2\,J_{\text{nom},11} \\ 0.2\,J_{\text{nom},11} & J_{\text{nom},22} & 0.2\,J_{\text{nom},11} \\ 0.2\,J_{\text{nom},11} & 0.2\,J_{\text{nom},11} & J_{\text{nom},33} \end{bmatrix} \tag{39}$$

where J_{bias} represents a constant bias matrix, accounting for the changes in inertia due to the target. Using this inertia matrix, the simulation was performed, and the results are illustrated in Figure 9.

The first observation is that, for the attitude tracking (Figure 9a), K_{INDI} no longer has the faster settling time. Moreover, both K_{INDI} and $K_{\text{INDI-FF}}$ present an underdamped response, with the former showing overshoot. Meanwhile, $K_{\text{INDI-MPC}}$ maintains a response with very little to none oscillations, presents no overshoot, and is still remarkably similar to that initially predicted by the MPC.

For the angular velocity (Figure 9b) and the torque (Figure 9c), the advantages of the MPC augmented INDI system become evident: the response presents *significantly smaller angular velocity peaks, and actuator usage* (see also Table 2). Compared to K_{INDI}, $K_{\text{INDI-FF}}$ presents less actuator usage and smaller angular velocity peaks, which is a direct consequence of its less aggressive attitude tracking. Nonetheless all three controllers are still capable of performing the detumbling maneuver with a large inertia bias.

6.2.2 Second Post-Capture Detumbling

For the second post-capture detumbling scenario, the inertia matrix is set as:

$$J_{\text{det}} = J_{\text{nom}} + 1.5\,J_{\text{bias}}, \tag{40}$$

where J_{bias} was defined in Eq. 39. This results in a 150% increase in the diagonal elements and substantial changes in the off-diagonal terms, with regard to the nominal inertia matrix. Using this modified inertia matrix, the simulation was performed, and the results are shown in Figure 10.

The benefits of the combined INDI & MPC approach become most evident in this simulation. In terms of attitude tracking (Figure 10a), it achieves by far the fastest settling time, with markedly reduced oscillations and overshoot. The angular velocity response (Figure 10b) shows substantially smaller peaks, while actuator usage (Figure 10c and Table 2) is drastically reduced — a direct result of the smoother attitude tracking and the constraints of Eq. 30.

Compared to K_{INDI}, the $K_{\text{INDI-FF}}$ controller exhibits improvements across all performance metrics but still remains significantly inferior to $K_{\text{INDI-MPC}}$. This does not imply that the feedforward filter could not be further refined to approximate the MPC performance; however, it can be easier to tune the MPC to obtain the desired performance given that it is an optimal control method, which is based on a model of the (closed-loop) plant and which offers intuitive tuning knobs in the form of the cost matrices in (33). Secondly, although both MPC and feedforward strategies can incorporate uncertainty in their design —— MPC through tube-based formulations and FF through robust tuning over a model set —— only MPC can guarantee an optimal response according to the defined cost function. Matching this level of optimality

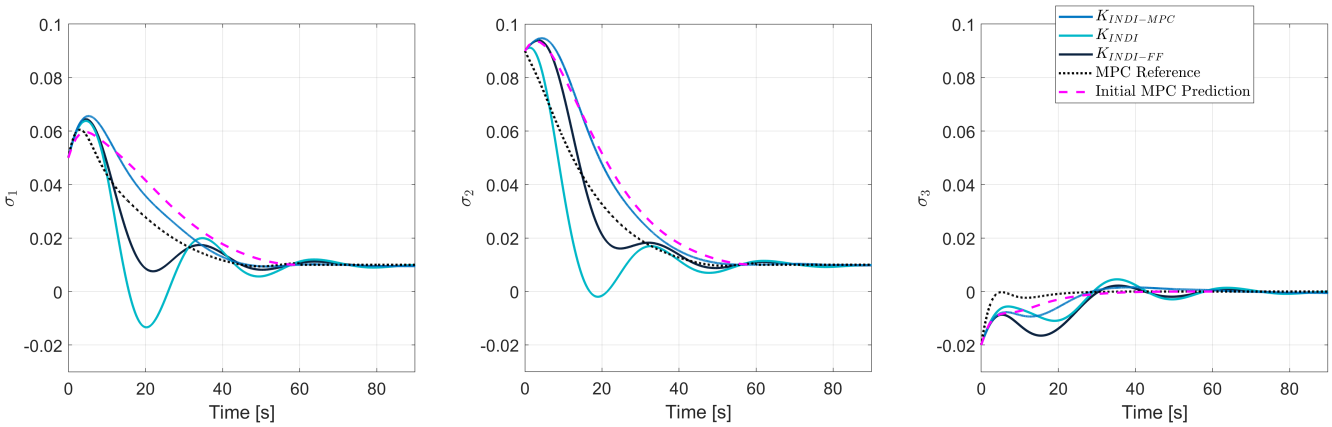

(a) Modified Rodrigues Parameters.

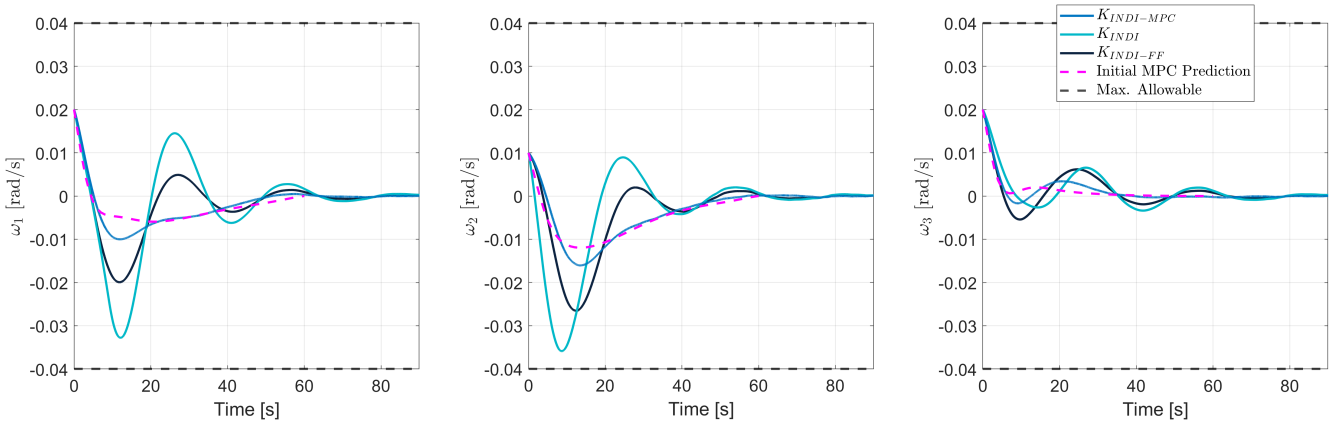

(b) Angular Velocity.

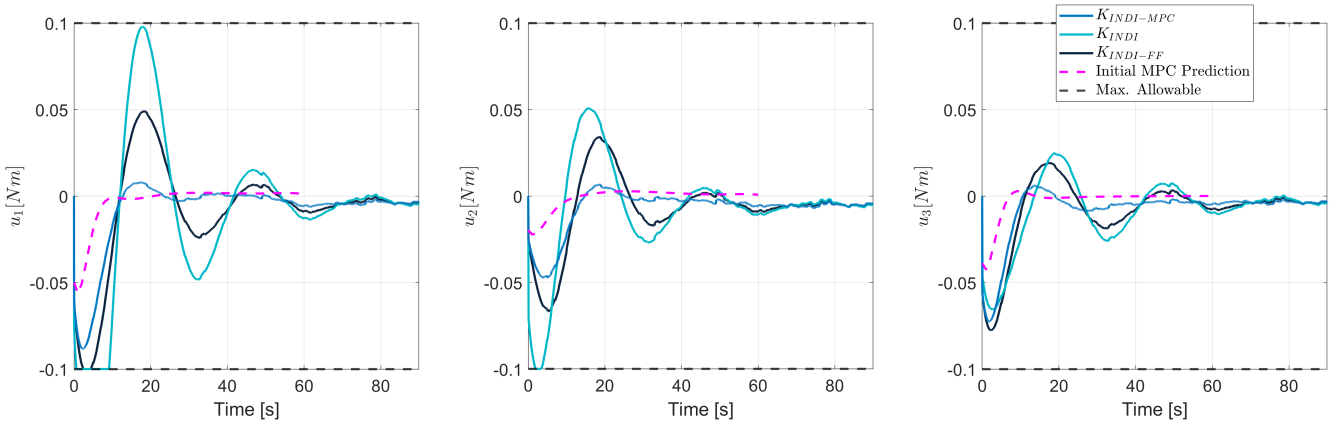

(c) Torque.

Fig. 9 Post-capture detumbling with inertia matrix $J_{\text{det}} = J_{\text{nom}} + J_{\text{bias}}$.

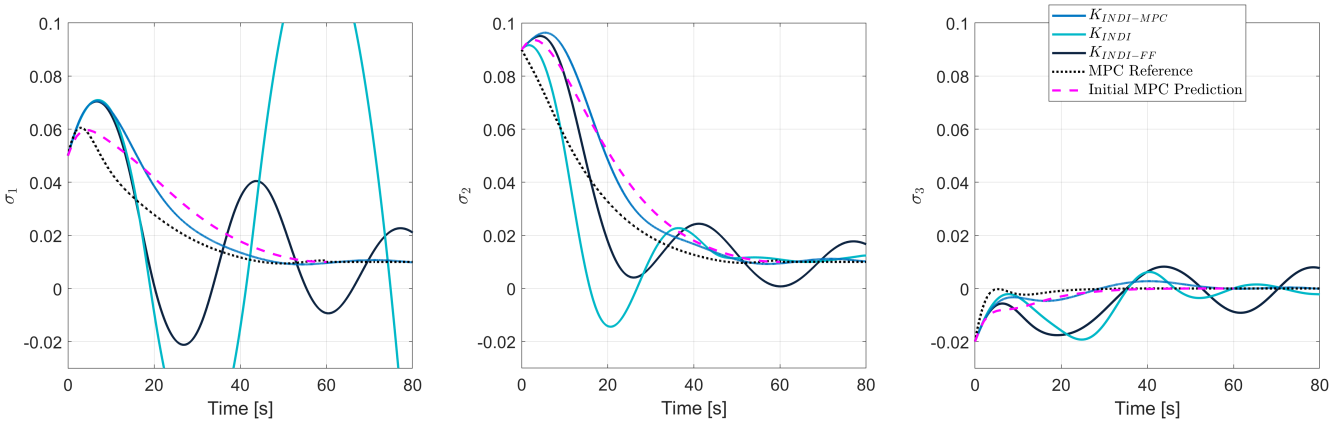

(a) Modified Rodrigues Parameters.

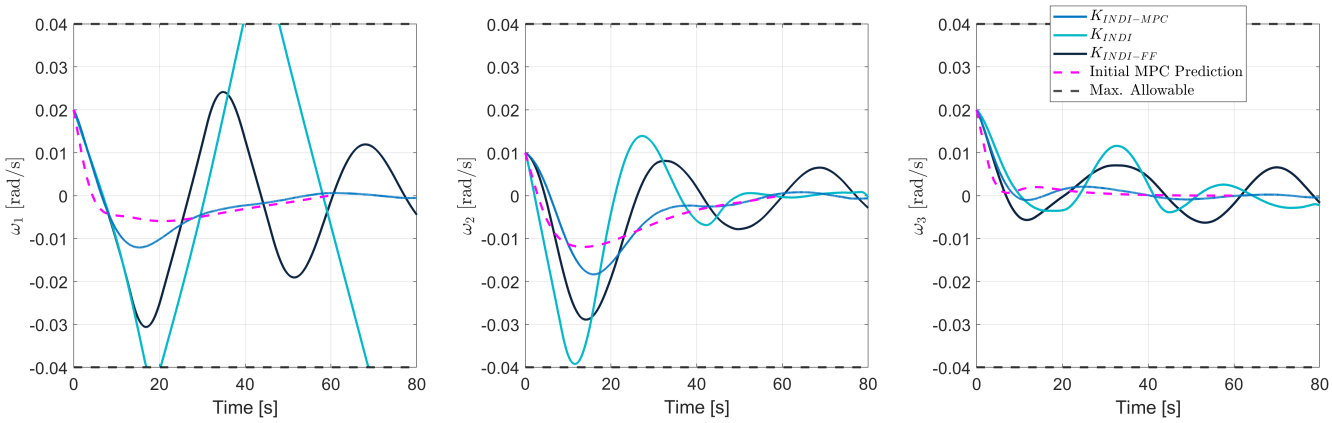

(b) Angular Velocity.

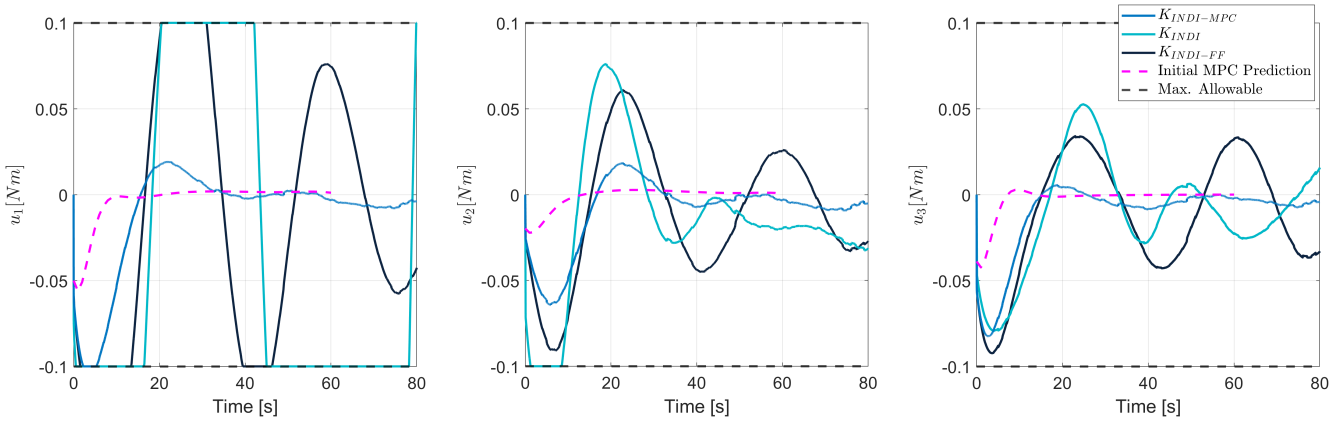

(c) Torque.

Fig. 10 Post-capture detumbling with inertia matrix $J_{\text{det}} = J_{\text{nom}} + 2\,J_{\text{bias}}$.

with a feedforward controller would demand a higher-order design and substantially greater tuning effort. Finally, another advantage of the MPC is that it can be easily reconfigured online; namely, the prediction model can be readily updated, e.g., in the case that an improved inertia estimate becomes available, thus adapting the guidance to the real mission conditions with minimal additional effort.

In this sense, the main advantage of the MPC strategy (when combined with the INDI approach) for spacecraft detumbling lies in its ability to provide an optimal response with low computational burden, while extending the range of operating conditions—both in terms of inertia and angular velocity—for which the controller remains effective. Moreover, the missionization effort required for MPC is significantly smaller than that for the feedforward approach: whereas the latter would likely require extensive retuning or gain scheduling to adapt to new mission conditions, the MPC framework would typically only require an adjustment of the enforced constraints.

7 Conclusion

A novel guidance and control framework for post-capture detumbling has been presented, combining robustly tuned INDI with MPC to address the challenges of large, uncertain inertia and strict actuator limits. Nonlinear simulations comparing K_{INDI}, $K_{\text{INDI-FF}}$, and $K_{\text{INDI-MPC}}$ show that while all controllers can stabilize the chaser–target system, the INDI & MPC approach consistently outperforms the others by achieving faster settling, smaller angular velocity peaks, lower actuator usage, and robust performance under uncertainty. This demonstrates the framework's ability to generate optimal, constraint-compliant responses with low computational effort.

The results highlight the practical advantages of the combined INDI & MPC methodology for post-capture operations and suggest a wider applicability across aerospace control problems. Future work will incorporate Robust MPC, namely Tube-Based MPC, to further enhance robustness and investigate the use of the proposed strategy for other aerospace scenarios, extending the benefits of this approach beyond the specific context of detumbling.

Acknowledgments

Part of this work was supported by national funds through Fundação para a Ciência e a Tecnologia, I.P. (FCT) under projects UID/50021/2025 and UID/PRR/50021/2025. The work of Afonso Botelho was supported by the Ph.D. Fellowship by the Portuguese Space Agency— Portugal Space through FCT, Portugal, under Grant PRT/BD/152809/2021.

Declaration of Use of Artificial Intelligence

AI was used to proofread this work.

References

[1] M. Oda. Space Robot Experiments on NASDA's ETS-VII Satellite: Preliminary Overview of the Experiment Results. In *Proceedings of the 1999 IEEE International Conference on Robotics and Automation (Cat. No. 99CH36288C)*, volume 2, pages 1390–1395. IEEE, 1999. doi: 10.1109/ROBOT.1999.772555.

[2] G. Hirzinger, K. Landzettel, B. Brunner, M. Fisher, C. Preusche, D. Reinsteema, A. Albu-Schaffer, G. Schreiber, and B.-M. Steinmetz. DLR's Robotics Technologies for On-Orbit Servicing. *Advanced Robotics*, 18(2):139–174, 2004. doi: 10.1163/156855304322758006.

[3] K. Yoshida, D. Dimitrov, and H. Nakanishi. On the Capture of Tumbling Satellite by a Space Robot. In *Proceedings of the 2006 IEEE/RSJ International Conference on Intelligent Robots and Systems*, pages 4127–4132. IEEE, 2006. doi: 10.1109/IROS.2006.281900.

[4] Y. Tincelin, A. Jozwicka-Perlant, D. Chipping, A. Caiazzo, I. Huertas Garcia, G. Visentin, R. Findlay, and A. Wolahan. Enabling a European In-Space Transportation Ecosystem. In *Aerospace Europe Conference 2023 – 10th EUCASS – 9th CEAS*, 2023. doi: 10.13009/EUCASS2023-759.

[5] S. Singh, E. Mooij, and D. Gransden. Multibody Approach to the Controlled Removal of Large Space Debris with Flexible Appendages. In *AIAA Scitech 2019 Forum*, page 1916, 2019. doi: 10.2514/6.2019-1916.

[6] S. Singh and E. Mooij. Robust Control for Active Debris Removal of a Large Flexible Space Structure. In *AIAA Scitech 2020 Forum*, page 2077, 2020. doi: 10.2514/6.2020-2077.

[7] F. Aghili. Optimal Control for Robotic Capturing and Passivation of a Tumbling Satellite with Unknown Dynamics. In *AIAA Guidance, Navigation, and Control Conference*. AIAA, 2008. doi: 10.2514/6.2008-7274.

[8] Shuang L. and Yuchen S. Recent Advances in Contact Dynamics and Post-Capture Control for Combined Spacecraft. *Progress in Aerospace Sciences*, 120:100678, 2021. ISSN: 0376-0421. doi: 10.1016/j.paerosci.2020.100678.

[9] F. Aghili. Time-Optimal Detumbling Control of Spacecraft. *Journal of Guidance, Control, and Dynamics*, 32(5):1671–1675, 2009. doi: 10.2514/1.43189.

[10] B. Zhang, B. Liang, Z. Wang, Y. Mi, Y. Zhang, and Z. Chen. Coordinated Stabilization for Space Robot after Capturing a Noncooperative Target with Large Inertia. *Acta Astronautica*, 134:75–84, 2017. doi: 10.1016/j.actaastro.2017.01.041.

[11] X. Huang, J. D. Biggs, and G. Duan. Post-capture Attitude Control with Prescribed Performance. *Aerospace Science and Technology*, 96:105572, 2020. ISSN: 1270-9638. doi: 10.1016/j.ast.2019.105572.

[12] L. Shi, J. Katupitiya, and N. Kinkaid. A Robust Attitude Controller for a Spacecraft Equipped with a Robotic Manipulator. In *2016 American Control Conference (ACC)*, pages 4966–4971, 2016. doi: 10.1109/ACC.2016.7526140.

[13] R. Rodrigues, V. Preda, F. Sanfedino, and D. Alazard. Modeling, Robust Control Synthesis and Worst-Case Analysis for an On-Orbit Servicing Mission with Large Flexible Spacecraft. *Aerospace Science and Technology*, 129, 2022. doi: 10.1016/j.ast.2022.107865.

[14] R. Rodrigues. Modeling, Robust Control Design and Analysis of Time-Varying Complex Space Missions Involving Large Flexible Structures. PhD thesis, Institut Supérieur de l'Aéronautique et de l'Espace (ISAE-SUPAERO), 2024.

[15] R. Rodrigues, F. Sanfedino, D. Alazard, V. Preda, and J. Olucha Delgado. Linear Parameter-Varying Gain-Scheduled Attitude Controller for an On-Orbit Servicing Mission involving Flexible Large Spacecraft and Fuel Sloshing. In *12th International Conference on Guidance, Navigation & Control Systems (GNC)*, Sopot, Poland, June 2023.

[16] J. Olucha Delgado. High-Accuracy Pointing Control during On-Orbit Satellite Refuelling. Master's thesis, TU Eindhoven (TU/e), 2023.

[17] H. Pfifer and E. Burgin. LPVTools 2.0 and its Application to Spacecraft Attitude Control. In *Proceedings ROCOND'2025/LPVS'2025*, 2025.

[18] P. Acquatella, W. Falkena, E. van Kampen, and Q. P. Chu. Robust Nonlinear Spacecraft Attitude Control using Incremental Nonlinear Dynamic Inversion. In *AIAA Guidance, Navigation, and Control Conference*, page pp. 4623, 2012. doi: 10.2514/6.2012-4623.

[19] P. Simplício, P. Acquatella, and S. Bennani. Design and Analysis of a Launcher Flight Control System Based on Incremental Nonlinear Dynamic Inversion. *Aerospace*, 12(4), 2025. doi: 10.3390/aerospace12040296.

[20] P. Simplício, M. Pavel, E. Van Kampen, and Q. P. Chu. An Acceleration Measurements-based Approach for Helicopter Nonlinear Flight Control using Incremental Nonlinear Dynamic Inversion. *Control Engineering Practice*, 21(8):1065–1077, 2013. doi: 10.1016/j.conengprac.2013.03.009.

[21] S. Sieberling, Q. P. Chu, and J. Mulder. Robust Flight Control using Incremental Nonlinear Dynamic Inversion and Angular Acceleration Prediction. *Journal of Guidance, Control, and Dynamics*, 33(6):1732–1742, 2010. doi: 10.2514/1.49978.

[22] T. Pollack. Advances in Dynamic Inversion-based Flight Control Law Design: Multivariable Analysis and Synthesis of Robust and Multi-Objective Design Solutions. PhD thesis, Technische Universiteit Delft, 2024. doi: 10.4233/uuid:28617ba0-461d-48ef-8437-de2aa41034ea.

[23] P. Acquatella. Agile Spacecraft Attitude Control: An Incremental Nonlinear Dynamic Inversion Approach. *IFAC-PapersOnLine*, 53, 2020. doi: 10.1016/j.ifacol.2020.12.1598.

[24] P. Acquatella, E. Van Kampen, and Q. P. Chu. A sampled-data form of incremental nonlinear dynamic inversion for spacecraft attitude control. In *AIAA SCITECH 2022 Forum*, 2022. doi: 10.2514/6.2022-0761.

[25] L. Encarnação. Tuning Hybrid Incremental Dynamic Inversion Control Laws Using $\mathcal{H}_\infty$ Loop-Shaping. Master's thesis, Technische Universiteit Delft, 2025.

[26] W. Van Soest, Q. P. C., and J. A. Mulder. Combined Feedback Linearization and Constrained Model Predictive Control for Entry Flight. *Journal of guidance, control, and dynamics*, 29(2):427–434, 2006. doi: 10.2514/1.14511.

[27] E. van Oort, Q. P. Chu, and J. A. Mulder. Nonlinear Robust Model Predictive Control for Lifting Body Re-Entry Flight Attitude Control. *IFAC Proceedings Volumes*, 40(7):323–328, 2007. doi: 10.3182/20070625-5-FR-2916.00056.

[28] J.J. Recasens, Q.P. Chu, and J.A. Mulder. Robust Model Predictive Control of a Feedback Linearized System for a Lifting-body Re-entry Vehicle. In *AIAA Guidance, Navigation, and Control Conference and Exhibit*, 2012. doi: 10.2514/6.2005-6147.

[29] D.A. Joosten. Constrained and Reconfigurable Flight Control. Doctoral thesis, TU Delft, 2017.

[30] T. Zhang. Nonlinear Incremental Optimal Control for Underactuated Mechanical Systems: Robust Tightly-Coupled NMPC and INDI applied to Underactuated Mechanical Systems. Master's thesis, TU Delft, Aerospace Engineering, Delft, The Netherlands, 2023.

[31] B. Wie. Space Vehicle Dynamics and Control. AIAA, 2nd edition, 1998. doi: 10.2514/4.860119.

[32] S. Wu, G. Radice, Y. Gao, and Z. Sun. Quaternion-based Finite Time Control for Spacecraft Attitude Tracking. *Acta Astronautica*, 69:48–58, 2011. doi: 10.1016/j.actaastro.2011.03.001.

[33] S. Skogestad and I. Postlethwaite. Multivariable Feedback Control: Analysis and Design. John Wiley & Sons, 2005. ISBN: 978-0470011683.

[34] C. Vlaar and G. Looye. Incremental Nonlinear Dynamic Inversion Flight Control. Master's thesis, Delft University of Technology, 2014.

[35] H. Khalil and J. Grizzle. *Nonlinear Systems*, volume 3. Prentice Hall Upper Saddle River, NJ, 2002. ISBN: 978-0130673893.

[36] J.J.E. Slotine and W. Li. Applied Nonlinear Control. Prentice Hall, Englewood Cliffs, NJ, 1991.

[37] B. Bacon, A. Ostroff, and S. Joshi. Nonlinear Dynamic Inversion Reconfigurable Controller utilizing a Fault Tolerant Accelerometer. In *19th DASC. 19th Digital Avionics Systems Conference. Proceedings (Cat. No. 00CH37126)*, 2000. doi: 10.1109/DASC.2000.884920.

[38] B. Bacon, A. Ostroff, and S. Joshi. Reconfigurable NDI Controller using Inertial Sensor Failure Detection & Isolation. *IEEE Transactions on Aerospace and Electronic Systems*, 37(4):1373–1383, 2001. doi: 10.2514/6.2000-4565.

[39] P. Acquatella. Robust Nonlinear Attitude Control of Aerospace Vehicles: An Incremental Nonlinear Control Approach. PhD thesis, Delft University of Technology, 2020. doi: 10.4233/uuid:99d82992-080c-4c5d-8d40-4e62e62285c0.

[40] X. Wang, E. van Kampen, Q. Chu, and P. Lu. Stability Analysis for Incremental Nonlinear Dynamic Inversion Control. *Journal of Guidance, Control, and Dynamics*, 42(5):1116–1129, 2019. doi: 10.2514/1.G003791.

[41] P. Acquatella, E. Van Kampen, and Q. P. Chu. A Sampled-Data Form of Incremental Nonlinear Dynamic Inversion for Spacecraft Attitude Control. In *AIAA SCITECH 2022 Forum*, 2022. doi: 10.2514/6.2022-0761.

[42] F. Grondman, G. Looye, R. Kuchar, Q P. Chu, and E. Van Kampen. Design and Flight Testing of Incremental Nonlinear Dynamic Inversion-Based Control Laws for a Passenger Aircraft. In *2018 AIAA Guidance, Navigation, and Control Conference*, page pp. 0385, 2018. doi: 10.2514/6.2018-0385.

[43] G. Papageorgiou. Robust Control System Design: $\mathcal{H}_\infty$ Loop Shaping and Aerospace Applications. PhD thesis, University of Cambridge, 1998. doi: 10.17863/CAM.19503.

[44] J. Rawlings, D. Mayne, and M. Diehl. Model Predictive Control: Theory, Computation, and Design 2nd Edition. Nob Hill Publishing, 2 edition, 2017. ISBN: 978-0-9759377-5-4.

[45] D. Malyuta, Y. Yu, P. Elango, and B. Açıkmeşe. Advances in Trajectory Optimization for Space Vehicle Control. *Annual Reviews in Control*, 52:282–315, 2021. ISSN: 1367-5788. Publisher: Elsevier BV. doi: 10.1016/j.arcontrol.2021.04.013.

[46] L. Blackmore. Autonomous Precision Landing of Space Rockets. *Bridge*, 46(4), 2016. ISSN: 07376278.

[47] N. Matni, A. Ames, and J. Doyle. A Quantitative Framework for Layered Multirate Control: Toward a Theory of Control Architecture. *IEEE Control Systems*, 44(3):52–94, June 2024. ISSN: 1066-033X, 1941-000X. doi: 10.1109/MCS.2024.3382388.

[48] Danylo Malyuta, Taylor P. Reynolds, Michael Szmuk, Thomas Lew, Riccardo Bonalli, Marco Pavone, and Behcet Acikmese. Convex Optimization for Trajectory Generation : A Tutorial on Generating Dynamically Feasible Trajectories Reliably and Efficiently. *IEEE Control Systems*, 42(5):40–113, Sept. 2022. ISSN: 1066-033X. doi: 10.1109/mcs.2022.3187542.

[49] Robin Verschueren, Gianluca Frison, Dimitris Kouzoupis, Jonathan Frey, Niels van Duijkeren, Andrea Zanelli, Branimir Novoselnik, Thivaharan Albin, Rien Quirynen, and Moritz Diehl. acados: a modular open-source framework for fast embedded optimal control. Oct. 2019. arXiv: 1910.13753.

[50] MOSEK ApS. *The MOSEK MATLAB API manual. Version 11.1.10.*, 2026.